Journal of Materials Chemistry A

Accepted Manuscript

ROYAL SOCIETY OF CHEMISTRY

www.rsc.org/materialsA

Journal Name

RSCPublishing

ARTICLE

Facile preparation of semimetallic MoP_2 as a novel visible light driven photocatalyst with high photocatalytic activity†

Cite this: DOI: 10.1039/x0xx00000x

Tianli Wu,[a] Shijian Chen,[a*] Dingke Zhang,[b] Junke Hou[c]

Received 00th January 2012,
Accepted 00th January 2012

DOI: 10.1039/x0xx00000x

www.rsc.org/

The production of clean and renewable H_2 by photocatalytic water splitting has attracted much attention due to increasing energy crisis. In this work, semimetallic MoP_2 nanoparticles are discovered as a new phocatalyst to efficiently degenerate methyl orange and produce H_2 from water under visible light irradiation. MoP_2 nanoparticles were prepared through solid-state reaction route via vacuum encapsulation technique following by acid washing. Both first-principle band-structure calculations and experimental measurements reveal a typical semimetallic characteristic of MoP_2. The obtained MoP_2 nanoparticles display superior photocatalytic performances of degradation of methyl orange with good stability and reduction of water assisted by sacrificial element Pt under visible light. The detection of hydroxyl radicals in the solution in presence of MoP_2 with fluorescence spectroscopy confirmed its photodegradable activities. The present study points out a new direction for developing semimetallic photocatalysts for the H_2 production through water splitting.

1. Introduction

Photocatalytic solar-energy conversion has received much attentions as a potential solution to the worldwide energy shortage and environmental degradation.[1-3] The search for suitable materials as photocatalysts using solar energy is one of the noble missions of material science. Hundreds of semiconducting materials have been explored as potential photocatalysts including oxides, nitrides, sulfides and phosphates. For example, $In_{1-x}NiTaO_4$ photocatalyst induces direct splitting of water into stoichiometric amounts of oxygen and hydrogen.[4] C_3N_4, an unconventional photocatalytic material, can generate H_2 from water even in the absence of noble metals as well as degrade organic contaminants.[5] Ni-decorated CdS nanorods can enhance photocatalytic H_2 generation by redox shuttle mechanism.[6] Ag_3PO_4 can harness visible light to decompose organic contaminants as well as oxidize water.[7] $Cu_2(OH)PO_4$ exhibits photooxidation properties in the near infrared range.[8] By far, TiO_2 is the most widely investigated and used photocatalyst due to its high photostability and efficiency.[9-13] The reported photocatalysts are mainly semiconductor which have been exclusively investigated in photocatalytic applications. Generally, light absorption across the band gap in semiconductors generates electron-hole pairs which subsequently migrate to the semiconductor surface to participate in redox reactions.[14] However, metallic materials differ from semiconductive materials in that there is no band gap separating between occupied and unoccupied levels, so they were believed to be useless for photocatalysis due to very fast recombination of photocarriers. Recently, the application potential of semimetallic materials as a novel and unconventional class of photocatalysts has been discovered. For example, Irvine et al., found a ternary compound, $Sr_{1-x}NbO_3$ as an effective photocatalyst and demonstrated that metallic perovskite oxides facilitate kinetic charge separation which is effective in decomposing methylene blue, as well as in photocatalytic hydrogen and oxygen evolution from water splitting.[15] Zhou et al, reported an elemental photocatalyst of black bismuth as a photocatalyst used to oxidize of NO in air and explained its photocatalytic mechanism from band structure.[16] At the same time, Dong et al, reported a semimetal bismuth element, which shows an impressive catalytic "memory" capability for the photocatalyst oxidation of NO in air and explained its photocatalytic activity and the catalytic "memory" of the Bi nanoparticles which could be ascribed to the UV-mediated surface plasmon resonance.[17] These discoveries provide new perspectives for photocatalyst research and thus motivated us to search for novel photocatalysts with metallic properties.

MoP_2 was reported as a semimetal and first synthesized by Rundqvist and Lundstroem in 1963.[18] As a semimetal, MoP_2 has unique properties, such as small effective masses, high carrier mobility, and a very small band overlap energy. In semimetallic materials, electron-hole pairs can be created by interband transitions where electrons are excited from the conduction band into the unoccupied energy levels in the higher band. And the high carrier mobility may allow carrier separation, especially if the carriers could be rapidly transferred.[15] In addition to its semimetallic property, we know very little.[19] Recently, Cho et al. synthesis MoP_2 by a mechanochemical reaction of Mo and P elements and reported its highly reversible Li-Ion intercalating MoP_2 nanoparticle cluster anode for lithium rechargeable batteries.[20] Here in, we synthesise

MoP_2 simply through solid-state reaction route via vacuum encapsulation technique following by acid washing. The material can harness visible light to decompose organic contaminants as well as generate H_2 from H_2O. An ab-initio density functional theory calculations indicate a semimetallic band structure, and the semimetallic characteristics of MoP_2 was confirmed by temperature dependent electrical transport measurements. Furthermore, OH radicals in aqueous solution detected by fluorescence spectroscopy confirms the photocatalytic activities of semimetallic MoP_2. Possible photocatalytic mechanism of semimetallic MoP_2 are discussed. We demonstrate MoP_2 nanoparticles as a promising and innovative photocatalyst for the H_2 production through water splitting.

2. Experimental procedure

2.1 Synthesis

MoP_2 nanoparticles used in this study were prepared through solid state reaction route in an evacuated sealed quartz tube followed by acid washing. High purity (~99.9%) Molybdenum oxide (MoO_3) and elemental red phosphorus (P) powders were used as molybdenum and phosphorus sources, respectively. First, 0.5g molybdenum oxide (MoO_3) and 0.4g red phosphorus (P) were mixed and vacuum-sealed (10E-5 Pa）in a quartz tube. Then, these sealed quartz tubes were placed in chamber furnace and heat treated at 850 ^oC for 3 hours (A) and 5 hours (C), respectively. Next, acid washing was performed afterwards to remove the impurities. The powders were transferred into a 50mL Teflon-lined stainless steel autoclave. The autoclave was filled with hydrochloric acid (15 wt%) to 80% of the total volume, tightly sealed and maintained at 200 ^oC in an air oven for 2 h. The final reaction products were thoroughly washed with deionized water and dried under 50 ^oC conditions.

2.2 Characterization

Powder X-ray diffraction analysis was measured by using a PANalytical X'pert diffractometer operating at 40 kV and 40 mA using Cu Kα radiation. The field emission scanning electron microscopy (FE-SEM, JEOL JSM-7800F) with an energy dispersive X-ray spectrometer (EDS) and a transmission electron microscopy (TEM Libra-200FE), were employed for the morphological observation, the size and structure of samples. Absorption spectra was measured on a Shimadzu UV-3600 spectrophotometer. The electrical resistivity was measured on a temperature dependent four point probe test system (Linseis LSR-3). The fluorescence spectra of the generated ˙OH adduct TAOH was measured on the fluorescence spectrophotometer at 425nm (Shimadzu RF-5301pc). Fluorescence was induced by excitation at 350nm. The changes of absorption at 465 nm were applied to identify the concentrations of MO using a spectrophotometer (Shimadzu UV-3600). The decolourization efficiency (η) of MO was calculated by $\eta\ (\%) = (1- C/C_0) \times 100\%$ where C and C_0 are concentrations of MO at visible irradiation time T and 0 min, respectively. Chemical oxygen demand (COD) was also measured at regular time intervals using COD tester (Lianhua Technology, 5B-3C). The mineralization efficiency of MO was estimated by mineralization of MO $(\%) = (1- COD/COD_0) \times 100\%$, where COD and COD_0 are the COD concentration of certain reaction time T and 0 min, respectively.

2.3 Photocatalytic degradation experiment

Photocatalytic degradation processes under visible irradiation (λ>400 nm) were carried out with the MoP_2 nanoparticles suspended in dye solution. The plane schematic diagram of reaction apparatus is shown (Fig. S1, ESI†). Many factors were considered on the influence of the decolorization efficiency of methyl orange, including catalyst dosage, pH, light intensity and initial concentration of dyes. In all cases, the solution was stirred continuously in the dark for 60 min to achieve adsorption/desorption equilibrium on the photocatalysts. The experiments have been performed at room temperature in order to eliminate temperature effects. Samples were withdrawn from the reactor every 15 min.

2.4 Photocatalytic hydrogen evolution from water

The hydrogen evolution experiments were carried out in a top-irradiation reaction vessel connected to a glass gas-closed circulation system. H_2 production was performed by dispersing 50 mg of MoP_2 powder in triethanolamine aqueous solution (50 mL, 20 vol.%). The 2 wt% Pt co-catalyst was photo-deposited on the MoP_2 catalyst by adding an appropriate amount of H_2PtCl_6 solution into the reaction solution. The light source was a 300 W Xenon lamp with a cut-off filter (λ>400 nm). The H_2 evolution was measured with an on-line gas chromatograph (GC9790II, FULI) with a thermal conductivity detector (TCD).

2.5 Detection of reactive species (hydroxyl radical, ˙OH)

Terephthalic acid (TA) can react with ˙OH forming highly fluorescent 2-hydroxyterephthalic acid (TAOH), the concentration of hydroxyl radicals was measured by the terephthalic acid (TA) fluorescence method. The mixture of 2E-3 molar of NaOH and 5E-4 molar of TA solution was prepared in deionized water. Then, 30 mg of the MoP_2 catalyst was dispersed in 50 mL of the TA aqueous solution. The solution was collected at every 15 min during the irradiation procedure in order to estimate the generated TAOH, which can be detected by fluorescence spectroscopy.

2.6 Theoretical calculations

All the calculations were performed at the generalized gradient approximation (GGA) of the Perdew-Burke-Ernzerhif (PBE) form[33] with the projector-augmented wave potentials implemented in the simulation package VASP.[34] The cut-off energy for the plane wave was chosen to be 500 eV and smearing was used with 0.5 eV. Monkhorst-pack k-points was set to be 7×7×7. The parameter of energetic convergence for self-consisted field is set as 10E-5 eV/atom. Moreover, the structural optimization of all ionic positions would finish until the Hellmann-Feynman (HF) forces were less than 0.01 eV/Å. Finally, for the calculation of the density of states (DOS) and energy band, a larger 9×9×9 k-point set was used.

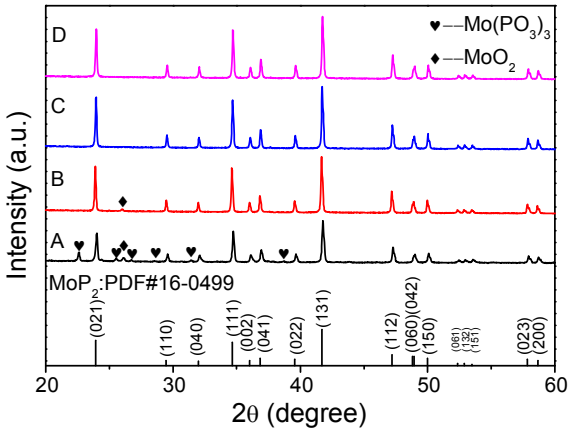

Figure 1. XRD patterns of MoP_2 prepared at different conditions. A: 3 hours reaction without acid washing; B: 3 hours reaction with hydrochloric acid washing; C: 5 hours reaction with hydrochloric acid washing; D: Sample C after photocatalytic test.

3. Results and discussion

3.1 Structure, morphology and compositions of MoP_2 nanoparticles

MoP_2 used in this study was prepared through solid state reaction route followed by acid washing. Figure 1 shows the XRD patterns of nanoparticles prepared at different conditions. Sample A was prepared in the quartz tube at 850 °C for 3 hours without acid washing. One can see most of the strong diffraction peaks can be indexed to orthorhombic structure of MoP_2 (JCPDS card no.16-0499). Except for those, some other weak diffraction peaks indexed to $Mo(PO_3)_3$ and MoO_2 are also observed, which indicates that the nanoparticles we obtained by reaction of MoO_3 and P under 850 °C are mixtures of MoP_2 with $Mo(PO_3)_3$ and MoO_2. In order to remove the impurities, the sample was treated with hydrochloric acid at 200 °C for 2 hours. After acid treatment, the absence of $Mo(PO_3)_3$ peaks in XRD pattern (B) indicates that $Mo(PO_3)_3$ has been successfully removed by acid washing. However, a weak peak of MoO_2 phase is still existed in the XRD pattern. The existence of MoO_2 in the sample might be due to incomplete reaction of MoO_3 and P. Therefore, we increased the solid-state reaction time from 3 to 5 hours and treated the sample with hydrochloric acid at 200 °C for 2 hours afterward. All the diffraction peaks in the XRD pattern (C) are indexed to MoP_2 (space group: Cmc21, JCPDS no. 16-0499) and the lattice constants are a = 3.145, b=11.184 and c=4.984 Å. The sharp and strong diffraction peaks indicate that the obtained MoP_2 is good crystalline. The above results indicate that high crystalline quality pure MoP_2 nanoparticles have been successfully prepared by solid-state reaction of MoO_3 and red phosphorus at 850 °C for 5 hours following by hydrochloric acid washing at 200 °C for 2 hours.

The field emission scanning electron microscopy (FESEM) images of the obtained pure MoP_2 sample are displayed in figure 2. The morphologies of MoP_2 look like capsules with different sizes and each capsule is composed of particles. The particles are uniformly distributed in the size range of several hundred of nanometers as shown in figure 2b. Energy dispersive X-ray spectrometer (EDS) analysis (inset of figure 2b) shows the atomic ratio of Mo : P is about 1 : 1.98, which indicates the synthesized MoP_2 is near the stoichiometric composition. Transmission electron microscopy (TEM) image provides further insight into the microstructure of the obtained particles, as shown in figure 3. The observed lattice fringes with a d-spacing of 0.192 nm and 0.217nm in the high-resolution TEM image, match well with the (112) and (131) crystal plane distance of MoP_2. Moreover, the product particles can be undoubtedly indentified as MoP_2 from their characteristic (021), (110), (131), (112), (200) and (062) reflections in the selected area electron diffraction (SAED) pattern (Figure 3b). These results also show that high quality crystalline MoP_2 nanoparticles have been synthesized.

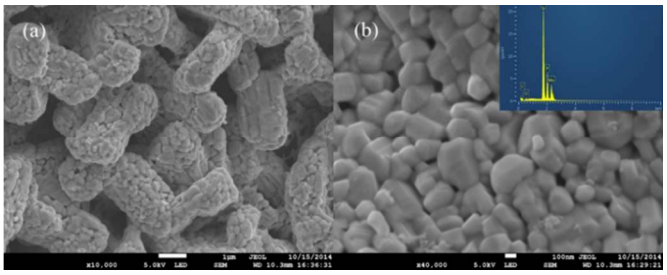

Figure 2. (a) Typical FESEM images from sample C MoP_2 powders shows capsule-like structures; (b)high magnification SEM images shows the capsule are composed of particles with hundreds nanometers in size; inset of (b) EDS spectra shows the atomic ratio of Mo : P is about 1 : 1.98.

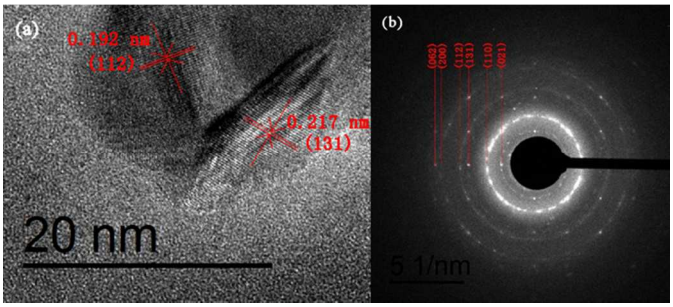

Figure 3. (a) HRTEM image of the MoP_2, (b) SAED of (a).

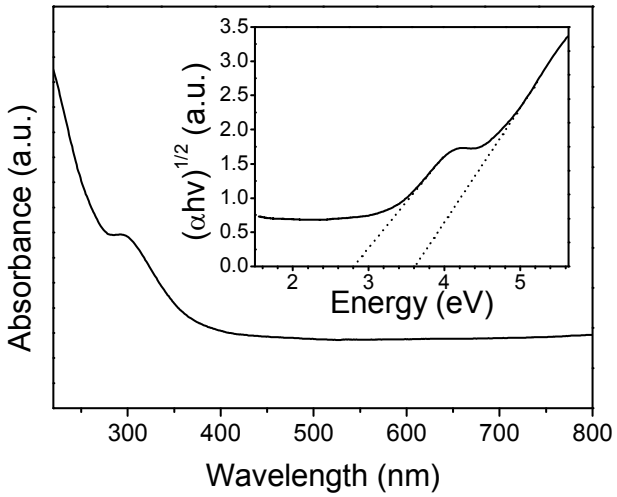

Figure 4. UV-vis absorption spectra of MoP_2 powder (inset: Kubelka- Munk transformed spectra).

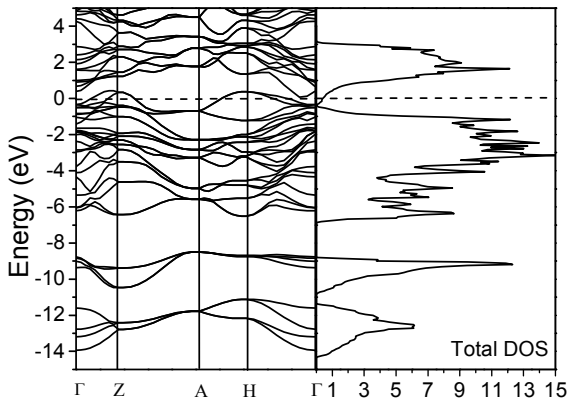

Figure 5. Calculated electronic band structure (left) and DOS (right) of MoP_2.

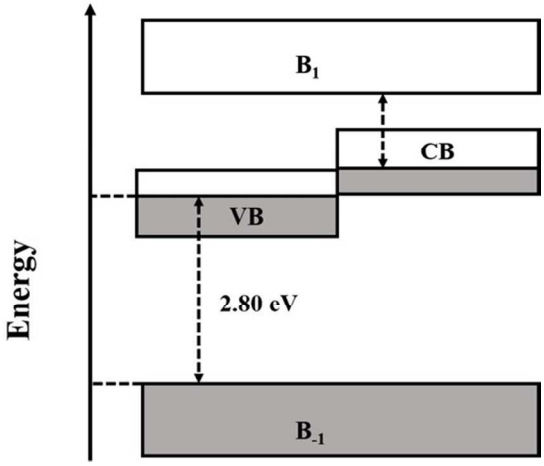

Figure 6. Schematic band structure of semimetallic MoP_2.

3.2 Optical properties and band structure

The absorption spectra in the wavelength range of 220-800 nm was measured to study the band structures of MoP_2, as shown in figure 3. The band gap energy of MoP_2 nanoparticles was obtained according to equation (1)[21]

$$(\alpha h\nu)^{1/n} = A(h\nu - E_g) \quad (1)$$

Where A is a proportionality constant, h is Planck's constant, ν is the frequency of vibration and α is an absorption coefficient. The value of n depends on the type of optical transition of the semiconductor ($n = 2$ for indirect transition).[22] The inset of figure 4 shows the $(\alpha h\nu)^{1/2}$ of MoP_2 as a function of the photon energy, and the absorption onsets are determined as 2.8 eV and 3.6 eV, respectively.

Performing density functional calculations, we theoretically study the electronic structures of MoP_2 nanoparticles. Figure 5 shows the calculated band structure and density of states (DOS) of MoP_2. For convenience, the Fermi level $E_f = 0$ is taken. It shows a small overlap between the bottom of the conduction band and the top of the valence band at Fermi level, which indicates a typical semimetallic characteristics. Our experimental measurement of electrical resistivity also show a linear dependence on the temperature from 30 °C to 550 °C and a slow increase of resistivity as the increasing temperature, which experimentally confirms the metallic conductivity of MoP_2 (Fig. S2, ESI†). Different from the well-described typical semiconductors, the valence band (VB) and conductive band (CB) of semimetallic MoP2 overlap. So, the strong absorption observed in the visible range and UV range cannot be explained on the basis of an electron transition from the occupied VB to the unoccupied CB. Zhou et al, present a possible mechanism to explain it in the research of semimetallic Bi.[16] They think the observed band gap can be assigned to the transition from an occupied level to the valence band. Along this line, we describe a corresponding schematic band structure of semimetallic MoP_2 which is shown in Figure 6. Based on our theoretical calculations, an indirect transition (2.3 eV) between the band below the VB and the VB (Figure 5) can be possible under visible light excitation. B_{-1} depicts the band below the VB, and B_1 depicts the band above the CB, respectively, as shown in Figure 6. According to this model, the observed band gap of 2.8 eV can be assigned to a B_{-1} to VB transition from an unoccupied level to the valence band. It should be noted that the experimental band-gap value (2.8 eV) is larger than the calculated value (2.3 eV) as a result of the well-known band gap underestimation.

A	Catalyst dosage (mg)	10	20	30	40	50
	Decolorization efficiency (%)	12	34	70	72	60
B	pH	2	4	6	8	10
	Decolorization efficiency (%)	84	96	79	8	4
C	Light intensity (mW cm^{-2})	11	18	24	34	43
	Decolorization efficiency (%)	73	89	100	100	100
D	Initial concentration (mg L^{-1})	5	10	15	20	25
	Decolorization efficiency (%)	93	100	87	84	76

Table 1. Parameters to the influence of decolorization efficiency of MO after 75 min visible light irradiation. A: Different MoP_2 dosage with the initial concentrations of MO (10 mg L^{-1}), pH=6.5, light intensity (24 mW cm^{-2}); B: Different pH with the initial concentrations of MO (10 mg L^{-1}), light intensity (24 mW cm^{-2}), MoP_2 dosage (30 mg); C: Different light intensity with the initial concentrations of MO (10 mg L^{-1}), pH=4, MoP_2 dosage (30 mg); D: Different initial concentrations of MO with pH=4, MoP_2 dosage (30 mg), light intensity (24 mW cm^{-2}).

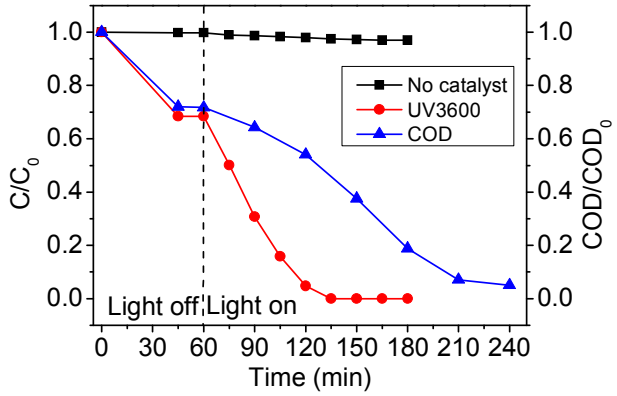

Figure 7. Decolourisation and degardation rate of methyl orange under visible light irradiation (λ>400 nm); initial MO concentration, 10 mg L^{-1}; catalyst dosage, 30 mg; pH, 4; light intensity, 24 mW cm^{-2}.

3.3 Photocatalytic degradation by MoP_2 nanoparticles

In order to investigate the photocatalytic activity of MoP_2 nanoparticles, the photodegradation of MO was carried out under visible light illumination. As we all know, many parameters can influence the decolorization efficiency of MO, such as catalyst dosage, pH, light intensity, initial concentration of dyes and so on. First, the above parameters have been systematically investigated and optimized which are shown in table 1. It has been shown that MoP_2 demonstrates the best degradation efficiency with a dosage of 30 mg (0.6 g L^{-1}), the MO initial concentrations of 10 mg L^{-1}, pH = 4, and light intensity of 24 mW cm^{-2} at 25 ^{o}C. Figure 7 shows the photodegradation progress of MO under visible light irradiation with above optimized parameters. One can see that about 30% decrease of MO after MoP_2 was added into the solution before turning on the light, which is due to the adsorption of MO onto MoP_2. After turning on the light, MO starts to decompose and almost 100% of MO has been quickly decolorized in 75 minutes. However, MO solution without adding MoP_2 is very stable against with light and has not been decolorized. MO, a representative of aze dyes, is hard to be degraded. Various photocatalysts have been investigated to remove MO under visible light irradiation. Channei *et al.*, reported photocatalytic decolorization of MO by Fe-doped CeO_2. The optimal decolorization efficiency of 3% Fe-doped CeO_2 is only 56% in 120 min under a light intensity of 185 mW cm^{-2}.[21] Wang *et al.*, reported Iron(III)-doped TiO_2 nanoparticles whose decolorization efficiency is about 65% in 120 min.[23] Ge *et al.*, reported photocatalytic degradation of MO by QDs sensitized CdS-Bi_2WO_6. The decolorization efficiency is about 100% in 180 min under 500W Xe lamp without no further adjustment of light intensity.[24] Cao et al., reported a compound of AgBr and Ag_3PO4 for decolorization of MO.[25] The decolorization efficiency is nearly 95.1% in 50 min under 500W Xe lamp. And very recently, Katsumata *et al.*, reported g-C_3N_4/Ag_3PO_4 composite for degradation of MO with very high degradation efficiency of 100% in 5 min under 300 W Xe lamp (λ>440 nm).[35] Considering the fact that the light intensity used in our work is relatively low, the photocatalytic efficiency of MoP_2 in present work is very high compared with the reported value in the literature. Apparently, the photocatalytic activity of MoP_2 with high efficiency has been discovered in our experiments.

Generally, decolorization measured by absorption spectra of MO does not mean that the dyes have been completely decomposed into harmless end products. It is a need to measure the amount of organic compounds in the solution during the photodegradation, which can been indirectly done by the chemical oxygen demand (COD) test. The COD test results are shown in figure 7. We can see it takes about 180 min to completely degrade organic contaminants which is slower than decolorization process. In the first 60 min of irradiation, over 95% of MO has been decolorized while COD removal is only 25%. There is only a small decrease of the COD due to the fact that MO molecules are firstly decomposed to lower molecular weight and colorless moleculer compounds and the resulting intermediates still contribute to the COD of the solution. However, after the decolorization of the MO solution, the COD decreases sharply reaching a plateau that corresponds to the oxidation of smaller uncolored compounds indicating that almost complete mineralization of intermediates has occurred.

To evaluate the photochemical stability of the catalyst, cyclic stability tests on MO solution degradation were examined (Fig. S3, ESI†). It is shown that the recycled MoP_2 sample is high durability and stability during the decolorized reaction. After 5 cycles of photocatalytic reaction, the activity of MoP_2 does not obvious drop, and the decolorization efficiency remaining 95% within 60 min visible light reaction. In addition, the final reaction products collected and dried under 50 ^{o}C condition were measured by XRD. As shown in figure 1, compared with the X-ray pattern of as-sythsized MoP_2, there is no obvious change after 5 cycles of photocatalytic reaction, which indicates MoP_2 exhibits good recycling stability with regard to photocatalytic performance. On the basis of all of the above results, the MoP_2 is discovered to be an effective photocatalytic active agent. Several factors may account for the enhanced photocatalysis of MoP_2 photocatalysts. First, the high activity of catalyst is related to the particle size and morphology of MoP_2 nanocrystals (see figure 2). It is well known that the particle morphology and sizes play an important role in photoactivity. Since the smaller crystals offer greater surface area to volume ratios and therefore enrich organic dyes and active species to the surface of MoP_2 nanoparticles to participate in the photocatalytic reactions. Moreover, the crystallinity of MoP_2 materials also plays a vital role in the degradative reaction. From the XRD analysis (see figure 1), the MoP_2 samples show high crystallinity, this might facilitate the transfer of the photoelectrons from bulk to surface and result in the rapid separation of photo-induced electrons and holes, leading to the generation of more active species.

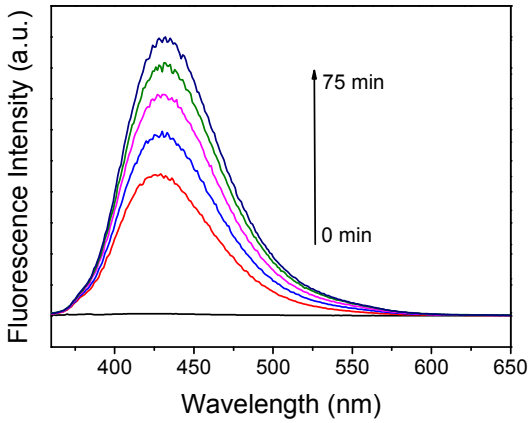

Figure 8. Fluorescence spectra of a TAOH solution generated by MoP_2 under visible light irradiation.

3.4 Generation of Hydroxyl radical (˙OH)

Hydroxyl radical, ˙OH, known as primary oxidant in the photocatalytic system, generated during the photocatalytic reaction and can be detected by a photoluminescence (PL) technique. The detection of hydroxyl radical (˙OH) in photocatalytic reactions have been reported by the reaction of terephthalic acid (TA) with ˙OH to generate highly fluorescent products, 2-hydroxyterephthalic acid (TAOH), which can be detected by fluorescence spectroscopy.[26]

The PL intensity of TAOH is proportional to the amount of ·OH produced during the photocatalytic reaction. As shown in Figure 8, the PL intensity at around 428 nm of TAOH increased with time, which means that ·OH radical increased continuously and TA was reacted to generate TAOH. The resulting ·OH radical, being a very strong oxidizing agent, can oxidize MO to the mineral end-products. The existence of hydroxyl radicals in the solution in presence of MoP_2 confirms the photocatalytic activities of MoP_2.

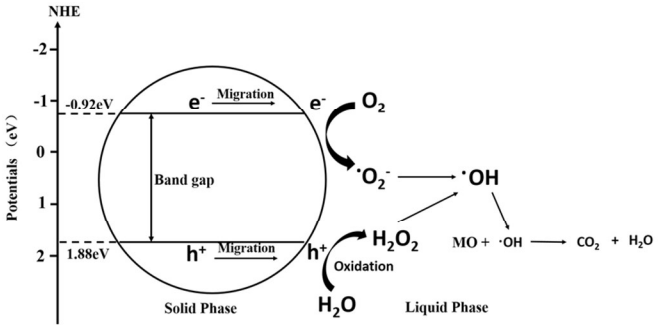

Figure 9. Possible proposed mechanism for the photoexcited electron-hole separation and transport processes under visible light irradiation.

3.5 Photodegradation mechanism analysis of MoP_2 photocatalysis

The mechanism of the semimetallic materials is still a riddle. Irvine et al. pointed out that metallic photocatalysts exhibit intermediate mechanisms compared to photoelectrocatalysts and photocatalysts.[15] According to the conventional mechanism of the semiconductor materials, we proposed a possible photocatalytic mechanism for MoP_2. Basing on the optical band gap energy values determined above (Figure 4) and equation (2) and (3) below, we can obtain the absolute energies of CB and VB of MoP_2.[27]

$$E_{cb}(MoP_2) = \chi(MoP_2) - E_c - \tfrac{1}{2}E_g \quad (2)$$

$$E_{vb}(MoP_2) = E_g - E_{cb}(MoP_2) \quad (3)$$

Where χ is the absolute electronegativity of the materials (χ is 4.98 eV for MoP_2[28]). E_c is the scaling factor relating the hydrogen electrode scale (NHE) to absolute vacuum scale (AVS) (~ 4.5 eV *vs.* AVS for 0 eV *vs.* NHE) and E_g is the band gap energy of MoP_2 (2.8 eV). The calculated CB and VB absolute energies of MoP_2 are -0.92 and 1.88 eV, respectively.

The proposed photocatalytic mechanism of MoP_2 can be seen in Figure 9, and the possible photocatalytic decomposition reactions are proposed as follows:

$$MoP_2 + h\nu \rightarrow MoP_2(e^- + h^+) \quad (4)$$

$$2H_2O + 2h^+ \rightarrow H_2O_2 + 2H^+ \quad (5)$$

$$H_2O_2 + e^- \rightarrow \cdot OH + OH^- \quad (6)$$

$$e^- + O_2 \rightarrow \cdot O_2^- \quad (7)$$

$$\cdot O_2^- + 2e^- + 2H^+ \rightarrow \cdot OH + OH^- \quad (8)$$

$$\cdot OH + MO \rightarrow\rightarrow H_2O + CO_2 \quad (9)$$

Firstly, the electrons are migrated from the B_{-1} to VB under visible light, leaving the holes behind. Secondly, the photo-excited electrons and holes are effectively collected by MoP_2 (eq (4)), so the recombination process of the electrons-hole pairs is hindered, and charge separation as well as stabilization is achieved. Thirdly, the H_2O can be oxidized to H_2O_2, then the H_2O_2 adsorbed on the surface of catalyst can be reduced to active species (eq (5) and eq (6)).[29] In addition, the O_2 adsorbed on the surface of catalyst can be reduced to active species (eq (7) and eq (8)).[30] The generated hydroxyl radical, ·OH, can react with the organic dye and generate degradation end-products (eq (9)).

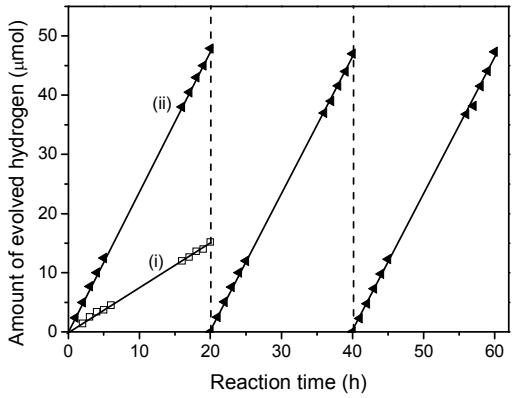

Figure 10. Stable hydrogen evolution from water by 50 mg MoP_2 catalyst. A time course of H_2 production from water containing 20 vol% triethanolamine as an electron donor under visible light (λ>400 nm) by (i) unmodified MoP_2 and (ii) ball-milling and 2.0 wt% Pt-deposited MoP_2 photocatalyst. The reaction was continued for 60 h, with evacuation every 20 h.

3.6 Hydrogen production from water

One of the most interesting properties of semiconductors where electrons and holes can be created by photo-irradiation is photocatalysis of reactions such as water splitting.[15] The photocatalytic H_2-production activity of synthesized MoP_2 nanoparticles was therefore investigated. And MoP_2 nanoparticles were shown to be photocatalytically active using visible light for reduction water splitting processes. The as-prepared MoP_2 nanoparticles achieved steady H_2 production from water containing triethnolamine as a sacrificial electron donor on light illumination (λ>400 nm), as shown in figure 10 (i). Control experiment showed no hydrogen evolution either in the dark or without pyhotocatalyst, indicating that the H_2 evolution proceeds in a photocatalytic way. These results demonstrate that MoP_2 nanoparticles play a role as a stable photocatalyst for visible-light-driven H_2 production. However, the H_2 evolution activity of MoP_2 nanoparticles was low and fluctuant, which might be due to large particles produced by high-temperature solid-state synthesis. This problem was solved by ball-milling nanoparticles and loading with a small amount of Pt, as described for other systems in the references. [15, 31, 32] The hydrogen production rate was increased from 15.2 umol/h/g photocatalyst to 47.3 umol/h/g after ball-milling and loading with 2 wt% Pt (Figure 10), which indicates that modified surface of MoP_2 nanoparticles and co-catalyst can significantly improve the photocatalytic activities. Continuous H_2 evolution with no obvious decrease of MoP_2 was clearly observed from the beginning of the reaction, indicating an excellent stability of the present material for photocatalytic H_2 production. H_2 production was also observed when other electron

donors were used instead of triethanolamine, such as methanol, oxalic acid, althought the H_2 evolution rates were lower (Fig. S3, ESI †). We estimated that the apparent quantum yield of photocatalytic hydrogen production is only 0.052% with monochromatic visible centred at a wavelength of 420 nm ($\Delta\lambda$= ±15 nm). Although the photocatalytic activity for the H_2 evolution is not very high comparing with other semiconductive photocatalyst, MoP_2 nanoparticles have shown promising and innovative potentials as an novel photocatalyst. Further work of water splitting and degrading other organic contaminants are under exploring.

4. Conclusions

In conclusion, semimetallic MoP_2 nanoparticles have been successfully prepared through solid state reaction route in an evacuated sealed quartz tube followed by acid washing. It is introduced as a new material type for the photocatalytic oxidation of MO in aqueous solution as well as production of H_2 from H_2O. The MoP_2 nanoparticles are capable of generating electrons and holes under visible light irradiation and quickly degrading organic contaminants. The detection of ·OH radical by the fluorescence spectroscopy provides clear evidence for this key property. These results open up a new avenue for the targeted development of semimetallic photocatalysts as new alternatives to conventional semiconductor materials.

Acknowledgements

This work is supported by the National Natural Science Foundation of China (NSFC) (grants 11304406 and 61307035). We also acknowledge the support from the sharing fund of large-scale equipment of Chongqing University.

Notes and references

* *Corresponding author*
[a]*School of Physics, Chongqing University, Shapingba, Chongqing 401331, China*
[b]*College of Physics and Electronic Engineering, Chongqing Normal University, Shapingba, Chongqing 401331, China*
[c]*Institute for Clean Energy & Advanced Materials, Faculty of Materials and Energy， Southwest University, Chongqing 400715, China*
Tel.: +86 23 65678362;
E-mail: sjchen@cqu.edu.cn

† Electronic Supplementary Information (ESI) available: schematic diagram of the photocatalysis reactor, Resistivity change with temperature, cycling runs of methyl orange decolourisation using pure MoP_2, H_2 production from water containing various electron donors under visible light. See DOI: 10.1039/b000000x/

1 A. Fujishima and K. Honda, *Nature* 1972, **238**, 37.
2 A. Kudo and Y. Miseki, *Chem. Soc. Rev.* 2009, **38**, 253.
3 H. Tong, S. Ouyang, Y. P. Bi, N. Umezawa, M. Oshikiri and J. H. Ye, *Adv. Mater.* 2012, **24**, 229.
4 Z. Zou, J. Ye, K. Sayama and H. Arakawa, *Nature* 2001, **414**, 625.
5 X. C. Wang, K. Maeda, A. Thomas, K. Takanabe, G. Xin, J. M. Carlsson, K. Domen and M. Antonietti, *Nat. Mater.* 2009, **8**, 76.
6 T. Simon, N. Bouchonville, M. J. Berr, A. Vaneski, A. Adrovic, D. Volbers, R. Wyrwich, M, Doblinger, A. S. Susha, A. L. Rogach, F. Jackel, J. K. Stolarczyk and J. Feldmann. *Nat. Mater.* 2014, **13**, 1013.
7 Z. G. Yi, J. H. Ye, N. Kikugama, T. Kako, S. Ouyang, H. Stuart-williams, H. Yang, J. Y. Cao, W. J. Luo, Z. S. Li, Y. Liu and R. L. Withers, *Nat. Mater.* 2010, **9**, 559.
8 G. Wang, B. B. Huang, X. C. Ma, Z. Y. Wang, X. Y. Qin, X. Y. Zhang, Y. Dai and M.-H. Whangbo, *Angew. Chem. Int. Ed.* 2013, **52**, 4810.
9 X. B. Chen, L. Liu, P. Y. Yu and S. S. Mao, *Science* 2011, **331**, 746.
10 R. Asahi, T.Morikawa, T. Ohwaki, K. Aoki and Y. toga, *Science* 2001, **293**, 269.
11 C. Y. Wang, D. W. Bahnemann and J. K. Dohrmann, *Chem. Commun.*, 2000, **16**, 1539.
12 J. M. Macak, M. Zlamal, J. Krysa and P. Schmuki, *Small* 2007, **3**, 300.
13 J. H. Choy, H. C. Lee, H. Jung and S. J. Hwang, *J. Mater. Chem.*, 2001, **11**, 2232.
14 X. B. Chen, S. H. Shen, L. J. Guo and S. S. Mao, *Chem. Rev.* 2010, **110**, 6503.
15 X. X. Xu, C. Randorn, P. Efstathiou and J. T. S. Irvine, *Nat. Mater.* 2012, **11**, 595.
16 Q. Zhang, Y. Zhou, F. Wang, F. Dong, W. Li, H. Li and G. R. Patzke., *J. Mater. Chem. A* 2014, **2**, 11065.
17 F. Dong, T. Xiong, Y. Sun, Z. Zhao, Y. Zhou, X. Feng and Z. Wu, *Chem. Commun.* 2014, **50**, 10386.
18 S. Rundqvist and T. Lundstroem, *Acta Chemi. Scand.* 1963, **17**, 37.
19 R. Ruhl and W. Jeitschko, *Monatsh. Chem.* 1983, **114**, 817.
20 M. G. Kim, S. lee and J. Cho, *J. Electrochem. Soc.* 2009, **156**, 89.
21 D. Channei, B. Inceesungvorn, N. Wetchakun, S. Ukritnukun, A. Nattestad, J. Chen and S. Phanichphant, *Sci. Rep.* 2014, **4**, 5757.
22 X. H. Wang, J.-G. Li, H. Kamiyama, Y. Moriyoshi and T. Ishigaki, *J. Phys. Chem. B* 2006, **110**, 6804.
23 J. M. Tarascon, *Nat. Chem.* 2010, **2**, 510.
24 L. Ge and J. Liu, *Appl. Catal. B: Environ.* 2011, **105**, 289.
25 J. Cao, B. Luo, H. Lin, B. Xu and S. Chen, *J. Hazard. Mater.* 2012, **217**, 107.
26 K. Ishibashi, A. Fujishima, T. Watanabe and K. Hashimoto, *Electrochem. Commun* 2000, **2**, 207.
27 Y. Xu and M. A. A. Schoonen, *Am. Mineral.* 2000, **85**, 543.
28 R. G. Pearson, *Inorg. Chem.* 1988, **27**, 734.
29 M. Yagi, K. Nagoshi and M. Kaneko, *J. Phys. Chem. B* 1997, **101**, 5143.
30 S. C. Yan, Z. S. Li and Z. G. Zou, *Langmuir* 2010, **25**, 3894.
31 B. Kraentler and A. J. Bard, *J. Am. Chem. Soc.* 1978, **100**, 4317.
32 M. Manikandan, T. Tanabe, P. Li, S. Ueda, G. V. Ramesh, R. Kodiyath, J. Wang, T. Hara, A. Dakshanamoorthy, S. Ishihara, K. Ariga, J. Ye, N. Umezawa and H. Abe, *Appl. Mater. Interfaces* 2014, **6**, 3790.
33 J. P. Perdew, J. A. Chevary, S. H. Vosko, K. A. Jackson, M. R. Pederson, D. J. Singh and C. Fiolhais, *Phys. Rev. B* 1992, **46**, 6671.
34 G. Kresse and J. Furthmuller, *Phys. Rev. B* 1996, **54**, 11169.
35 H. Katsumata, T. Sakai, T. Suzuki and S. Kaneco, *Ind. Eng. Chem. Res.*, 2014, 53, 8018.